crystals

MDPI

Article

Influence of Deposition Temperature on the Mechanical and Tribological Properties of Cr/Ni Co-Doped Diamond-like Carbon Films

Hassan Zhairabany [1,*], Hesam Khaksar [2], Edgars Vanags [3], Anatolijs Šarakovskis [3], Enrico Gnecco [2] and Liutauras Marcinauskas [1,4,*]

[1] Department of Physics, Kaunas University of Technology, Studentų Str. 50, 51368 Kaunas, Lithuania
[2] M. Smoluchowski Institute of Physics, Jagiellonian University, ul. Lojasiewicza 11, 30-348 Krakow, Poland
[3] Institute of Solid State Physics, University of Latvia, Kengaraga Str. 8, LV-1063 Riga, Latvia; anatolijs.sarakovskis@cfi.lu.lv (A.Š.)
[4] Plasma Processing Laboratory, Lithuanian Energy Institute, Breslaujos Str. 3, 44403 Kaunas, Lithuania
* Correspondence: hassan.zhairabany@ktu.edu (H.Z.); liutauras.marcinauskas@ktu.lt (L.M.)

Abstract

This study aimed to examine the influence of sputtering temperature on the bonding structure and properties of non-hydrogenated chromium/nickel co-doped diamond-like carbon (DLC) films synthesized via direct current magnetron sputtering. The Cr/Ni doping levels in the coatings were regulated by varying the shield opening above a chromium-nickel (20/80 at.%) target, resulting in a total metal co-doping concentration ranging from 6.1 to 8.9 at.%. The thickness of the Cr/Ni-DLC films ranged from 160 to 180 nm. Meanwhile, the deposition temperatures of 185 °C and 235 °C were achieved by adjusting the substrate-to-target distance. The XPS and Raman spectroscopy results indicated enhanced graphitization of the Cr/Ni-DLC films with a decrease in the synthesis temperature. XPS results indicated the formation of carbon-oxide and metal-oxide bonds, with no evidence of metal carbide formation in the doped DLC films. Furthermore, both the nanohardness and Young's modulus demonstrated significant improvement, while the friction coefficient was reduced more than twice as the deposition temperature increased. These findings provide valuable insights into the influence of deposition temperature on Cr/Ni co-doped DLC films, highlighting their potential as advanced functional coatings.

Keywords: Cr/Ni-DLC; microstructure; friction coefficient; nanohardness; deposition temperature; nano-scratching

Academic Editor: Hiroshi Yokoyama

Received: 11 December 2025
Revised: 31 December 2025
Accepted: 7 January 2026
Published: 12 January 2026

1. Introduction

Diamond-like carbon (DLC) films have attracted wide attention due to their outstanding mechanical and tribological properties, such as a relatively low coefficient of friction, high hardness and elevated elastic modulus. These characteristics make DLC coatings promising for diverse applications in mechanical systems, microelectronics and optical and biomedical devices [1–4]. However, several critical drawbacks limit the broader use of DLC coatings as protective coatings: limited microstructure modification, ductility and toughness, high internal stress, insufficient adhesion, thermal stability, etc. [5–7]. Pure DLC coatings demonstrate a high hardness, but can be brittle, non-ductile and experience a high compressive stress originating from the dense sp^3-rich carbon network, which can cause

cracking, pealing or delamination, limiting the long-term durability of DLC coatings in practical environments as protective layers [1,4,7].

To improve the mechanical and tribological properties, thermal stability and reduce the internal stress of the DLC films, researchers have explored elemental doping strategies, as metal or non-metal dopants can modify the carbon bonding structure by changing the ratio of sp^2 and sp^3 carbon bonds, creating metal nanocrystals, metal carbides or metal oxide in the carbon matrix. Consequently, the micro-hardness, ductility, toughness, conductivity and wear resistance will be improved; the friction coefficient and internal stress will be reduced in the doped DLC coatings [2,7]. It was demonstrated that various carbide-forming metals (Cr, Ti, Mo, W) and non-carbide-forming metals (Ag, Ni, Au, Cu) are widely used as dopants for controlling the sp^2/sp^3 bond ratio and improving the properties of DLC coatings [2,7–9]. Chromium and nickel are of particular interest: Cr is widely used to reduce the friction coefficient and improve the adhesion, wear, ductility and corrosion resistance of DLC films, although it often decreases hardness and promotes the conversion of sp^3 to sp^2 sites. Also, the formation of the chromium carbide phase in the carbon matrix could act as a solid lubricant, lowering the friction coefficient [2,4,10–16]. Ni doping can reduce internal stress and modify the microstructure of DLC films, but it also tends to increase sp^2 bonding, which may weaken hardness while improving toughness and ductility. Additionally, the presence of Ni metallic nanoparticles and higher sp^2 content in DLC films reduce the friction coefficient, improves electrical conductivity and corrosion resistance [2,7,15,17–19]. Importantly, the final properties of Cr-DLC and Ni-DLC films depend strongly on the dopant concentration and synthesis conditions [11–13,15,17].

Recently, more and more research has been directed towards improving the structure and properties of DLC coatings by incorporating not just a single dopant [20–29], but several chemical elements as co-dopants. Due to the synergy of the two chemical elements introduced, it is possible to obtain DLC coatings whose properties and microstructure can be changed in a significantly wider range compared to a single-element doped DLC films [9,27,30]. For instance, W. Dai et al. [31] demonstrated that silicon and oxygen co-doping enhanced adhesion strength and tribological performance of DLC films compared to the Si-doped film. X. Li et al. [21] reported that the multi-element alloy doping increased the hardness and reduced the friction coefficient of DLC films, due to the formation of a metal carbide phase and a higher sp^3 bond fraction. B. Mi et al. [22] highlighted that the rise in the titanium content in Cr/Ti-DLC films led to the growth of the TiC phase, reduced the sp^3 sites fraction and enhanced the corrosion resistance. R. Zhang et al. [29] observed that the increase in the Cr concentration in a-C:B:Cr films increased the sp^2 bond fraction but also reduced the friction coefficient of the films at moderate Cr concentration. Y. Zhang et al. [32] demonstrated that the hardness was improved with the addition of boron in the Ni/B-DLC films. Additionally, a slightly lower friction coefficient was obtained due to an increased fraction of sp^3 bonds. It was demonstrated that the increase in Cr concentration in the Cr/Ag co-doped DLC films enhanced the hardness up to 51% compared to pure DLC, due to the formation of the Cr-C phase, despite a reduction in the sp^3 bond fraction [25]. L. Sun et al. [24] observed that the larger Cr/Cu concentrations induced structural ordering and stipulated the formation of C=C bonds, Cr-C phase and cooper oxidation, which caused a reduction in the hardness, the surface energy and allowed control of the surface roughness of DLC films. C. Zhou et al. [33] demonstrated that the increase in Cr content from 1.1 to 10.4% enhances the sp^2 bond fraction and leads to the formation of Cr-C phase in Cr/F-DLC films. It was found that the friction coefficient, wear rate and corrosion resistance of the Cr/F-DLC films could be controlled by modulation of the Cr concentration. Y. Wu et al. [26] observed that an increase in the total Si/Ni concentration in the DLC films enhanced the oxygen content and the sp^3 C-C fraction, leading to lower H/E and H^3/E^2

values. Y. Xiao et al. [27] indicated that by controlling the Ni/N ratio in the DLC films, it is possible to reduce the friction coefficient two-fold and enhance the hardness by 18% due to the transition from sp^2-C to sp^3-C with an increase in nitrogen content. A. Zarei et al. [30] found that the rise in the Ni concentration allows for controlling the sp^2/sp^3 sites ratio and improving the optical properties due to optimal Ni and N concentrations in the Ni/N-DLC films. The synthesis of DLC coatings, binary doped with Ni and Cr, was performed using magnetron sputtering and pulse cathodic arc. The addition of Ni/Cr reduced the amount of sp^3 C-C bonds, which led to the lower hardness and enhanced the friction coefficient from 1.8 to 2.7 times compared to the undoped DLC coating. However, the total concentration of the Ni/Cr metals in the amorphous carbon films was very high and varied from 54.4 to 59.0 at.% [34]. It should be highlighted that most authors studied the tribological properties of Ni-DLC, Cr-DLC and co-doped DLC coatings at the macro-scale regime. In the meantime, there has been a lack of research on the tribological properties of co-doped DLC films using nanoscale loads (up to 100 nN). There is no data on how the structure, mechanical and nanotribological properties of DLC coatings will be affected with a low Cr/Ni concentration and what will be the effect of the synthesis temperature on the properties of Cr/Ni co-doped DLC films prepared by magnetron sputtering.

Another key factor is deposition temperature, which influences atomic mobility, dopant incorporation and sp^2/sp^3 bond ratio during film growth. At elevated temperatures (of less than 300 °C), DLC coatings can suffer from oxidation, graphitization and delamination, which severely degrade performance [35]. To overcome these issues, researchers have studied multilayer architectures and elemental doping at controlled deposition temperatures as strategies to reduce the friction coefficient, internal stress, enhance film durability and mechanical properties [10,23,36]. L. Sun et al. [23] indicated that Cu/Cr co-doped DLC films deposited at 250 °C achieved an ultra-low friction coefficient (less than 0.11) and increased hardness values compared to non-doped DLC films. B. Huang et al. [32] demonstrated that the increase of the formation temperature from 120 °C to 180 °C reduced the hardness and tribological properties of the Si-DLC films due to the rise in sp^2 C=C bond fraction. Despite the chromium or nickel co-doping of various DLC films with others chemical elements, such as Cr/N, Cu/Cr, Cr/Ti, B/Cr, Cr/Ag, Ni/B, B/Ni/CNT, Si/Ni and Ni/N, being used and demonstrating promising results for tailoring the structure and enhancement of properties, the co-doping of DLC films with Cr/Ni has still barely been investigated. Additionally, there is no data on the influence of deposition temperature on the microstructure of Cr/Ni-DLC films.

In this work, hydrogen-free Cr/Ni co-doped DLC thin films were prepared by direct current magnetron sputtering at temperatures of 185 °C and 235 °C. The mechanistic understanding was provided of how moderate deposition temperatures and low-level Cr/Ni co-doping affected the chemical composition, bonding structure, oxygen/metal bonding states, mechanical and nanotribological properties of DLC films. This study highlights the deposition temperature as an effective tool for tailoring the sp^2 and sp^3 carbon bond fraction and oxidation level, thereby achieving advanced Cr/Ni-DLC coatings with tunable performance for next-generation protective applications.

2. Experimental Section

2.1. Films Formation

The chromium and nickel co-doped non-hydrogenated diamond-like carbon (Ni/Cr-DLC) films were prepared on a silicon (100) substrate using the direct current magnetron sputtering deposition technique in an argon ambient. The substrate–target distance was used to manipulate the deposition temperature. The films were prepared at 4 cm and 8 cm distances, which allowed the substrates to reach temperatures of 235 °C and 185 °C,

respectively. Two flat magnetron targets (graphite and nickel/chromium) were utilized, with a graphite (99.9% purity) and a nickel/chromium target consisting of 80% Ni and 20% Cr (99.99% purity, Testbourne Ltd., Helmond, The Netherlands). The currents for the graphite and Ni/Cr targets were maintained at 1.5 A and 0.25 A, respectively. A shield with a controlled width was placed above the Ni/Cr target to manage the flux of sputtered chromium and nickel atoms. The co-doped DLC films' deposition was carried out at 4 mm (2.92 cm^2) and 8 mm (5.84 cm^2) of shield opening, and the synthesis duration was kept at 10 mm. The shield has a rectangular shape with a fixed length of 73 mm, and its width was selected at 4 mm and 8 mm. During the formation of the co-doped DLC films, the Si substrate moved forward and backward over the magnetron targets to have a homogenous distribution of the metal dopants. Detailed information about the deposition process and chamber setup is available in our previous articles [9,28].

2.2. Characterization Techniques

Energy dispersive X-ray spectroscopy (EDX) (Bruker Quad 5040 spectrometer, Hamburg, Germany) was used to determine the carbon and dopants' atomic concentrations. The elemental composition was determined by averaging measurements from five distinct points, utilizing an accelerating voltage of 10 kV and a magnification of 100. The thicknesses of doped DLC films were determined by a profilometer. The step height between a coated region and an uncoated Si substrate was measured at least three times at different points on each film and average values were calculated. Raman spectroscopy was used to study the microstructure of the Cr/Ni-DLC films. Raman spectra were obtained by a Renishaw inVia microscope system (Wotton-Under-Edge, UK) at an excitation wavelength of 532 nm. Three measurements were performed for each co-doped DLC film using 0.3 mW beam power and 10 s exposure duration. The spectra were measured in the 100–2000 cm^{-1} range (resolution of 0.8 cm^{-1}). The obtained spectra were analyzed using a Gaussian function to determine the D and G peak positions and calculate the D and G peak intensity ratio (I_D/I_G). X-ray photoelectron spectroscopy (Escalab 250XI, ThermoFisher, Waltham, MA, USA) was used to determine the elemental composition and bonding state. Prior to the measurements, the surfaces of samples were cleaned by Ar+ gun sputtering, the ion energy fixed at 2.0 keV for 30 s and the cleaned area was 4 mm^2. The detailed information about the carbon bonds and metal states (Ni and Cr) in the films was obtained from the XPS spectra in the ranges of 280–290 eV, 850–885 eV and 570–590 eV, respectively. Atomic force microscopy (AFM) measurements were completed to obtain the surface roughness and nanofriction behavior of the films using DriveAFM (Nanosurf, Liestal, Switzerland). The nanotribological measurements were done using a PPP-LFMR probe, the normal load was changed from 10 to 45 nN, the track length was <30 μm, the sliding velocity was kept at 52 μm/s, and single-pass scans were used [9,28]. The measured data acquisition and image analysis were evaluated by Gwyddion software. MTS-Agilent G200 nanoindenter (MTS Systems, Eden Prairie, MN, USA) was used for nanohardness measurements. The detailed measurement conditions are listed in our previous study [9,28]. In addition, a commercial DriveAFM (Nanosurf, Liestal, Switzerland) was employed to scratch the films, by applying load forces ranging from 3 μN to 7 μN over a scratch length of 5 μm. For both scratching and subsequent imaging, a diamond-coated AD-40-AS probe (Adama Innovations Ltd., Dublin, Ireland) with a spring constant of 26.41 N/m was used. All measurements were conducted under ambient conditions (relative humidity of 21% and a temperature of 23 °C). The scratching process was performed in the interlaced mode, where the AFM cantilever moves in a single direction. Initially, the Cr/Ni-DLC films were scratched, followed by imaging using the tapping mode. The depth and width of scratched grooves on the films were determined.

3. Results and Discussion

3.1. Elemental Composition and Bonding Structure

Tables 1 and 2 demonstrate the elemental composition results obtained from EDX and XPS measurements, respectively. It should be noted that the EDX data represents the averaged values across the entire doped DLC bulk films and substrate (later the silicon content was eliminated after normalizing the values to show only the coating content). However, the XPS measurements provide data limited to a few layers on the surface (about a few nanometers). The two trends that can be seen in the EDX results are: firstly, the increase in the deposition temperature from 185 °C to 235 °C, resulting in a lowering of the Ni and Cr content in both films. Secondly, this increase in the deposition temperature led to an increase in the oxygen concentration in both coatings. This tendency can be linked to the breakdown of the DLC matrix, which shifts toward a softer structure and a non-crystalline arrangement, facilitating increased oxygen integration. The average thickness of the Cr/Ni-DLC41 and Cr/Ni-DLC82 films was 170 nm. The lowest thickness of 160 nm was observed for the Cr/Ni-DLC81 film, while the thickness of the Cr/Ni-DLC42 film was ~180 nm.

Table 1. EDX results of the Cr/Ni-DLC films.

Samples *	Reached Temperature During Deposition (°C)	C (at.%)	O (at.%)	Ni (at.%)	Cr (at.%)
Cr/Ni-DLC81	185	85.1 ± 2.3	6.0 ± 1.1	5.7 ± 0.3	3.2 ± 0.1
Cr/Ni-DLC82	185	83.6 ± 2.1	8.6 ± 1.3	5.1 ± 0.2	2.7 ± 0.2
Cr/Ni-DLC41	235	87.8 ± 2.4	6.1 ± 1.2	4.0 ± 0.1	2.1 ± 0.1
Cr/Ni-DLC42	235	81.2 ± 1.9	12.2 ± 1.4	4.5 ± 0.2	2.1 ± 0.1

* First digit "4" refers to deposition temperature 235 °C, "8" to 185 °C and second digit "1" relates to shield opening area 2.92 cm^2, "2" to 5.84 cm^2.

Table 2. XPS results of the Cr/Ni-DLC films.

Samples	Reached Temperature During Deposition (°C)	C (at.%)	O (at.%)	Ni (at.%)	Cr (at.%)
Cr/Ni-DLC81	185	79.0	17.2	3.1	0.7
Cr/Ni-DLC82	185	75.8	19.7	3.7	0.8
Cr/Ni-DLC41	235	84.6	13.9	1.2	0.3
Cr/Ni-DLC42	235	73.6	18.9	6.1	1.4

Table 2 summarizes the surface composition of Cr/Ni-DLC films obtained by XPS. The oxygen content increased from 17.2 to 19.7 at.% for films deposited at a lower temperature, with the increase in shield width from 4 mm to 8 mm, respectively. Additionally, an increase in the Cr and Ni concentrations in the Cr/Ni-DLC82 film was observed. Meanwhile, the oxygen content was enhanced from 13.9 to 18.9 at.% when the deposition of the Cr/Ni-DLC films was performed at a higher temperature. The wider slit width resulted in a higher concentration of the Cr (1.4 at.%) and Ni (6.1 at.%) in the DLC film (Table 2). As residual oxygen molecules are present in the deposition chamber, slight oxidation occurs in the Cr/Ni-DLC coatings during deposition.

The XPS results demonstrated that the films exhibit a higher oxygen content than indicated by the EDX measurements. This difference in the oxygen concentrations is mainly attributed to the oxidation of the surface when the Cr/Ni-DC films were exposed to the air environment. Also, the difference in the metal and oxygen concentrations is due to the detection nature between the used techniques mentioned earlier, as the surface layers of the DLC films are more contaminated with oxygen. The existence of oxygen in the W and Ti co-doped DLC films is ascribed to contamination, poor vacuum conditions

and other factors [37]. L. Sun et al. [24] indicated that the enhancement in the total Cr and Cu content increased the oxygen concentration and stipulated the appearance of carbon-oxygen and metal oxide sites in the Cu/Cr-DLC coatings. The observed increase in oxygen concentration within the films is attributed to contamination occurring during the synthesis process. B. Zhou et al. [38] observed that the a-C:NiCr coatings contained from 2.6 to 3.4 at.% of oxygen, which is attributed to the atmospheric oxygen, when the vacuum chamber was depressurized. Y. Wu et al. [26] found that the oxygen content in the Si/Ni-DLC and Si/Ta-DLC films was from 13.0 to 20.9 at.%, respectively. Therefore, the oxygen content was minimized from 20.9 to 4.65 at.% after etching 20 nm of film. It was stated that the existence of a relatively high concentration of oxygen is due to absorption in the air. Meanwhile, the actual concentration of oxygen in these DLC coatings can range from 3 to 5%, depending on the dopant type and concentration. C. Zhou et al. [33] stated that the existence of oxygen in the Cr/F-DLC coatings was due to the oxygen residual in the vacuum chamber and the oxidation of the films upon exposure to the atmosphere. A.A. Solovyev et al. [19] observed that the Ni-DLC coating consisted of 16 at.% of oxygen when the Ni content was ~25 at.%. The emergence of nickel oxides was related to the existence of oxygen in the vacuum chamber.

The fitted C 1s spectra of the Cr/Ni-DLC films are given in Figure 1, where the extracted C-C peak, C=C peak and carbon-oxygen bond areas data after the fitting procedure are listed in Table 3. The sp^2/sp^3 bond ratios discussed in this work are derived from XPS C 1s peak deconvolution (Table 3). The results indicated that the peak distributions range from 283.9 eV to 284.1 eV in Figure 1a–d. The distribution of carbon bonding states led to a minor shift difference between the spectra of each coating.

Table 3. Extracted data from C 1s spectra of the Cr/Ni-DLC films.

Samples	C=C sp^2		C-C sp^3		C-O and C=O		Ratio
	Position, eV	Area, %	Position, eV	Area, %	Position, eV	Area, %	sp^2/sp^3
Cr/Ni-DLC81	283.8	47.45	284.7	39.46	286.9	13.09	1.20
Cr/Ni-DLC82	283.8	50.89	284.9	41.42	287.4	7.69	1.23
Cr/Ni-DLC41	283.9	43.52	284.8	43.30	287.0	13.18	1.01
Cr/Ni-DLC42	283.7	50.59	284.6	43.03	287.2	6.47	1.18

The XPS spectra were fitted into three individual bands located at ~283.9 eV, ~284.8 eV and ~287.0 eV and were assigned to C=C (sp^2), C–C (sp^3) and C=O bonds, respectively [23,39]. Following the theoretical prediction of C=C and C-C peak positions, the energy difference between these two bands was set to ~0.9 eV; a similar fitting method was used in the literature [40]. Notably, in some studies, an additional peak attributed to nickel carbide (Ni-C) or chromium carbide (Cr-C) could be found at ~282.8 eV [22,25,38]. Several authors demonstrated that the doping or co-doping of the DLC films with the carbide-forming metals (Mo, Cr, Ti, etc.) could lead to the appearance of a metal carbide peak in the range of 283.5–282 eV [22,25,34]. However, the Ni-C or Cr-C peaks were not detected in the XPS spectra of our Cr/Ni-DLC films (Figure 1).

It was obtained that the sp^2 C=C bond area increased from 43.5% to 50.6%, while the C-O and C=O bond area was reduced from 13.2% to 6.5% when the Cr/Ni concentration was increased in the DLC films deposited at a 235 °C temperature, respectively (Table 3). As a result, the sp^2/sp^3 ratio in the films deposited at a 235 °C temperature increased from 1.01 to 1.18 when the shield opening was widened from 4 to 8 mm, respectively. Meanwhile, the reduction in the synthesis temperature led to the formation of the Ni/Cr-DLC films with a relatively higher sp^2/sp^3 bond ratio. The sp^2 C=C bond and sp^3 C-C bond areas were 47.5% and 39.5% for the Cr/Ni-DLC81 film, respectively. A slight rise in the Cr/Ni

amount (according to XPS data) resulted in an enhancement in the peak areas of the sp^2 and sp^3 sites in the Cr/Ni-DLC82 film (Table 3). However, the carbon oxygen sites area in the Cr/Ni-DLC82 film was reduced by 40%, despite the oxygen concentration being higher compared to the Cr/Ni-DLC81 film. The results indicated that the sp^2/sp^3 ratio shifted to a slightly higher value from 1.20 to 1.23. The XPS data demonstrated that the sp^2/sp^3 ratio in the Cr/Ni-DLC films was slightly reduced when the deposition temperature increased from 185 to 235 °C. It was found in our previous study [9] that the increase in the amount of Mo resulted in a higher concentration of sp^2 sites. This trend is achieved when looking at the sp^2/sp^3 value of Cr/Ni-DLC81 film (1.20), which has a higher Cr and Ni content compared with the Cr/Ni-DLC41 film, which has a lower sp^2/sp^3 value of 1.01. As the oxygen content in the films prepared at the same shield opening was quite similar, the main factor influencing the reduction in the sp^2/sp^3 ratio is the higher deposition temperature of the Cr/Ni-DLC films. B. Zhou et al. [34] found that the sp^2 to sp^3 bond ratio in the Cr/Ni-DLC coatings depended on the Ni to Cr concentration ratio, and higher metal concentrations resulted in a higher sp^2 C=C fraction.

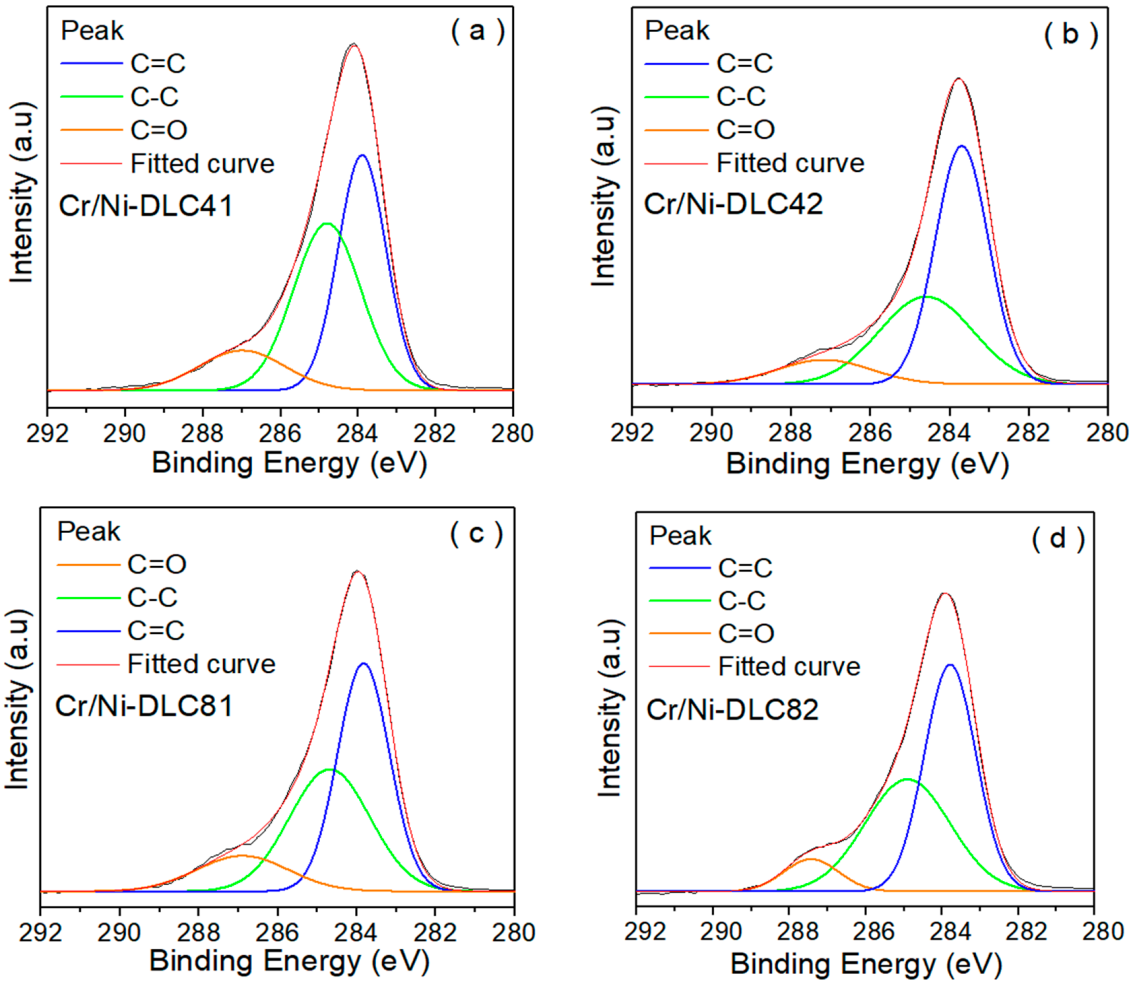

Figure 1. Fitted C 1s spectra of (**a**) Cr/Ni-DLC41; (**b**) Cr/Ni-DLC42; (**c**) Cr/Ni-DLC81; and (**d**) Cr/Ni-DLC82 films. (First digit "4" refers to deposition temperature 235 °C, "8" to 185 °C, and second digit "1" refers to shield opening area of 2.92 cm^2, "2" to 5.84 cm^2).

The higher fraction of sp^2 C=C bonds in the Cr/Ni-DLC42 film compared to Cr/Ni-DLC41 is due to two main reasons. The larger the shield width, the more Cr and Ni atoms could reach the substrate, resulting in an increased Cr/Ni content (from 1.5 to 7.5% by XPS data). The enlargement in Cr/Ni dopant concentration will enhance the oxygen

concentration in the coatings. The elemental composition data demonstrated that the oxygen amount was higher in the Cr/Ni-DLC42 film. It is well known that the doping of DLC films with Cr or Ni metals can inhibit the growth of sp^3 bonds and facilitate the appearance of sp^2 clusters. C.W. Zou et al. [13] demonstrated that the increase in the Cr concentration from 3.0% to 9.7% in the DLC films stimulated the conversion of sp^3 C-C sites to sp^2 carbon bonds. Y. Wu et al. [26] demonstrated that an enhancement in Ni/Si concentrations promoted the reduction in the sp^2/sp^3 ratio, but more C-O sites were formed in the DLC coatings. L. Sun et al. [23] observed that the increase in Cu/Cr amount in the DLC films enhanced the formation of the metal oxide bonds. Oxygen preferentially bonds to sp^2 carbon sites by creating the carbonyl or carboxyl groups in the DLC films. These bonds break the continuous sp^3 C-C network and increase the sp^2 clustering in the DLC coatings doped with metals [9,15,26].

The Cr2p and Ni2p spectra for the Cr/Ni-DLC films prepared at 8 cm of shield opening and different temperatures are given in Figure 2. The broad band situated at ~576 eV is attributed to the Cr-O bonding sites (Cr^{3+} states) in the films. It was observed that the presence of Cr-Cr and Cr-C bonds is ascribed to the peaks located in the range of 574–575 eV in the Cr doped DLC films [10–12] and Cr/F-DLC films [33]. It is likely that due to the sufficiently high oxygen content, the metallic chromium and chromium carbides were not formed in our films. The XPS spectra of the Cr2p demonstrated that all chromium was bonded only with oxygen and existed as Cr_2O_3 in the formed Cr/Ni-DLC films.

Ni2p core level spectra of Cr/Ni-DLC films were fitted with four peaks to determine the bonding states of the nickel (Figure 2a,b and Table 4). The band located at ~852.2 eV is assigned to metallic Ni (Ni^0) clusters formed in the carbon matrix. The peaks situated at ~854.5 eV and ~858–859 eV are due to the nickel oxide bonds of Ni^{2+} and Ni^{2+}/Ni^{3+} chemical states of Ni $2p_{3/2}$ core level, respectively. While the peak found in the range of 861–862 eV is related to the formation of the Ni/Ni^{2+} satellite in the DLC coatings containing nickel [17,26,27,34]. H. Zhou et al. [38] found that the existence of the bands at 854.4 eV and 859 eV in Ni-DLC films is assigned to the Ni-O bonds due to contamination in the air. The different chemical affinities and valence states of Ni and Cr contribute to the observed bonding behavior in the Cr/Ni-DLC films. Nickel exhibits a relatively narrow valence stability, predominantly favoring the Ni^{2+} state, which promotes the formation of metallic Ni-Ni clusters and Ni-O bonds in the presence of oxygen. In the meantime, the chemical affinity for the carbon atom is weak, and the formation of the nickel carbide phase in the Ni-doped DLC films is generally unlikely [26,34,38]. In contrast, chromium exhibits several stable valence states (Cr^{2+}, Cr^{3+} or Cr^{6+}) and its chemical affinity to carbon is higher compared to oxygen. Therefore, in most chromium-doped DLC coatings, the formation of Cr-C bonding in the carbon network dominates over Cr-O formation [16,22,25]. In the present Cr/Ni-DLC films, the preferential formation of Ni-Ni, Ni-O and Cr–O bonds, along with the absence of metal carbide phases, was observed. The absence of Cr-C phases could be due to the relatively low Cr concentration in the Cr/Ni-DLC coatings. It was stated that Cr-C bonds are formed when the Cr concentration is 3–5 at.% [13].

Table 4. Extracted data from Ni 2p spectra of the Cr/Ni-DLC films.

Samples	Ni (Ni^0)		NiO (Ni^{2+})		Ni Oxides (Ni^{2+}/Ni^{3+})		Ni/Ni^{2+} Satellite	
	Position, eV	Area, %	Position, eV	Area, %	Position, eV	Area, %	Position, eV	Area, %
Cr/Ni-DLC81	852.35	29.0	854.49	51.1	858.91	12.4	861.76	7.5
Cr/Ni-DLC82	852.20	27.4	854.50	50.1	859.40	16.1	862.30	6.4
Cr/Ni-DLC41	852.96	39.6	854.80	28.5	856.90	15.1	860.80	16.8
Cr/Ni-DLC42	852.00	30.5	854.30	46.8	858.20	10.6	861.10	12.1

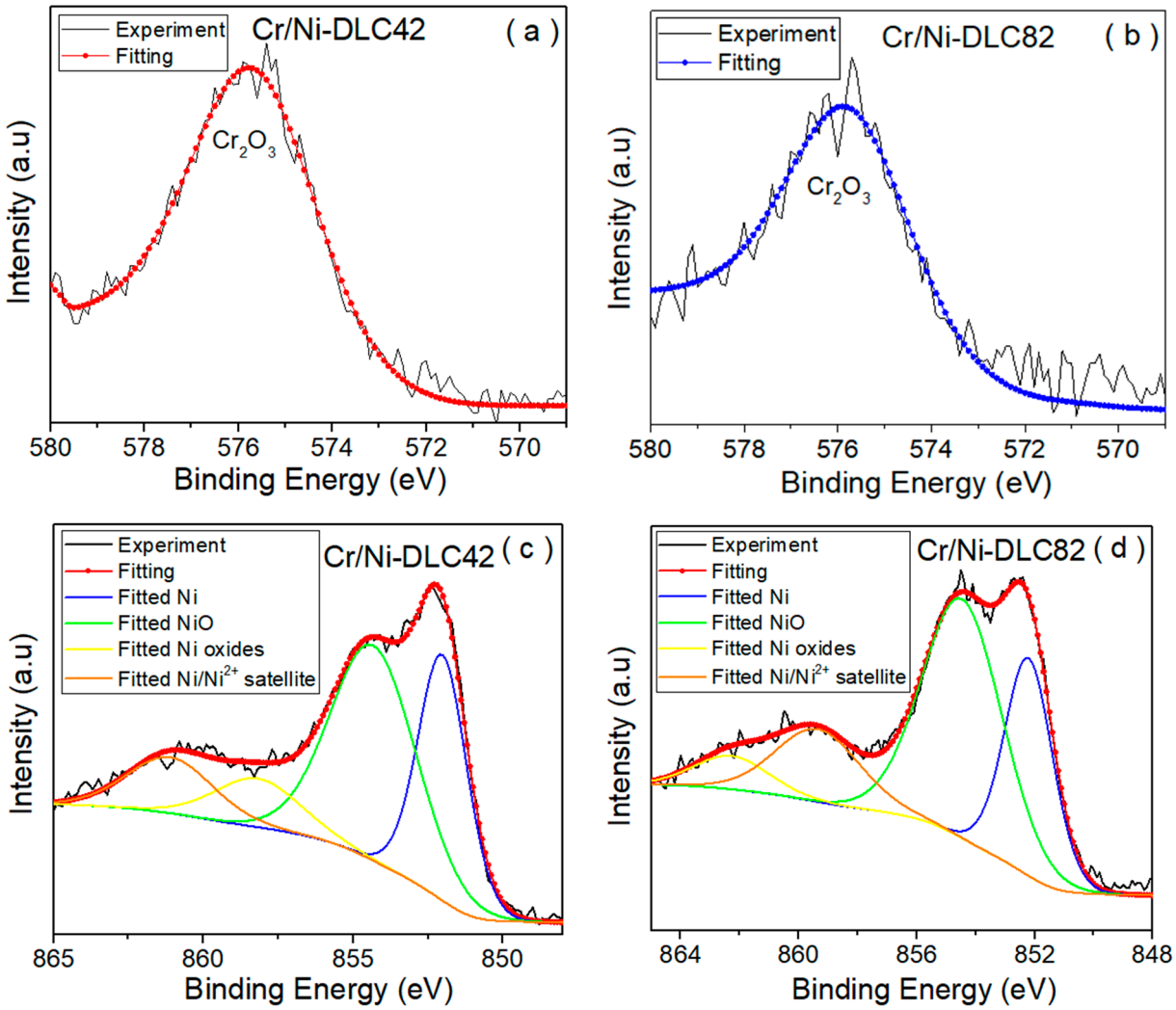

Figure 2. The XPS spectra of Cr/Ni-DLC42 (**a**,**c**) and Cr/Ni-DLC82 (**b**,**d**) films: (**a**,**b**) Cr2p and (**c**,**d**) Ni2p spectra.

The XPS data confirmed that nickel atoms during deposition do not bond with carbon or chromium atoms but react with oxygen atoms to create nickel oxide bonds. Meanwhile, part of the nickel atoms will form metallic clusters in the amorphous carbon matrix. It was found that the increase in the Cr/Ni concentration in DLC films deposited at 235 °C resulted in a reduction in the peak area related to the metallic nickel from 39.6% to 30.5%. Y. Wu et al. [26] determined that DLC films with higher Ni and Si concentrations contained more oxygen and the fraction of metallic nickel in the films was reduced. The fraction of metallic nickel in the Cr/Ni-DLC films formed at 185 °C was lower than that in the Cr/Ni-DLC films deposited at 235 °C (Table 4).

In addition, oxygen incorporation was higher when the deposition was performed at lower temperatures, where it partially bonds with carbon (C–O, C=O), nickel (NiO) and chromium (Cr_2O_3) and disrupts the tetrahedral carbon network, promoting the formation of sp^2 domains. Since both Ni and Cr are known graphitization catalysts that promote sp^2 clustering, thus it is logical that the Cr/Ni-DLC41 film with the lowest content of metals will have the highest values of the sp^3 C-C sites. At higher temperatures, the oxygen preferentially binds to Ni and Cr, forming stable oxides (Ni–O, Cr–O), which reduces its detrimental effect on the sp^3 carbon framework. Meanwhile, at lower temperatures, the probability of having a higher fraction of carbon-oxygen bonds increases [9,10]. Increasing the target-to-substrate distance reduces the kinetic energy of the sputtered carbon,

chromium and nickel atoms due to the increased path length and the number of collisions the atoms must undergo before arriving at the Si substrate. Longer sputtering distances will enhance the probability of metal and carbon atoms interacting with the oxygen, resulting in the formation of a higher fraction of carbon-oxygen, chromium-oxygen and nickel-oxygen sites inside the doped DLC films. It was stated that the metal atoms with lower kinetic energy typically show increased oxidation during the sputtering process. At a lower target-to-substrate distance, the arriving Cr and Ni atoms will have higher kinetic energy and could induce structural defects in the carbon network by breaking the bonds between the atoms. These structural defects will serve as additional nucleation centers of the sp^3 hybrid phase. This will result in relatively higher amounts of sp^3 C-C bonds in Cr/Ni-DLC films, even at higher synthesis temperatures [16]. Increasing the width of the shield above the Cr/Ni target increases the flux of sputtered metal atoms reaching the Si substrate, while causing minimal variation in their kinetic energy. Consequently, higher concentrations of Ni and Cr are incorporated and higher oxidation degrees are achieved in the DLC films (Tables 2 and 4). The slightly higher metal atom fluxes can indirectly reduce the diffusion length of adatoms on the surface, resulting in only minor structural changes (a reduction in the sp^2/sp^3 ratio and the formation of more carbon-oxygen and Ni-O bonds) at the same deposition temperature. In addition, the oxygen content detected by XPS was insignificantly lower in the Cr/Ni-DLC films deposited at higher temperatures than in those at lower temperatures (Table 2). The total fraction of the Ni-O bonds in the Cr/Ni-DLC-81 and Cr/Ni-DLC-82 films was 71.0% and 72.6%, respectively.

Figure 3 presents the fitted Raman spectra of all Cr/Ni-DLC films. The Gaussian fitting was performed to determine the D and G peaks' positions in the Raman spectra. Despite that, the Raman spectroscopy does not provide numerical values of the sp^2/sp^3 ratio; two important parameters can assess the variation trends of the sp^2 and sp^3 bonds within the films, these are the intensity ratio (I_D/I_G) and the integrated area ratio (A_D/A_G) of D and G peaks listed in Table 5. Additionally, the Raman spectra of the Cr/Ni-DLC films were used to assess structural disorder and graphitic clustering induced by the addition of Cr/Ni and oxygen.

Table 5. The main parameters of Raman spectra of the Cr/Ni-DLC films.

Samples	D Peak Position (cm^{-1})	$FWHM_D$ (cm^{-1})	G Peak Position (cm^{-1})	$FWHM_G$ (cm^{-1})	I_D/I_G	A_D/A_G	D′ Peak Position (cm^{-1})	O Peak Position (cm^{-1})
Cr/Ni-DLC81	1392.3	152.1	1552.6	115.1	0.49	0.66	1611.9	1695.3
Cr/Ni-DLC82	1393.2	166.2	1546.2	118.7	0.52	0.73	1612.2	1687.8
Cr/Ni-DLC41	1406.6	295.2	1559.9	139.2	0.62	1.31	---	---
Cr/Ni-DLC42	1409.1	281.3	1556.9	136.9	0.59	1.26	---	---

Considering the difference in the detection through the film's thickness between EDX and XPS, where the information obtained from Raman spectroscopy is from the entire thickness of the film. The I_D/I_G and A_D/A_G ratios in the Cr/Ni-DLC41 films were 0.62 and 1.31, respectively. The increase in metal concentration led to a slight reduction in the I_D/I_G (0.59) and A_D/A_G (1.26) ratios of the Cr/Ni-DLC42 film. However, the FWHM of G peak values were 139 and 137 cm^{-1} for Cr/Ni-DLC41 and Cr/Ni-DLC42 films, respectively. Additionally, the G peak shifted to lower wavenumbers from ~1560 to 1557 cm^{-1}. This shift in the G band indicates an increase in disorder and oxidation of sp^2 carbon sites [15,41]. The increase in the metal content resulted in a narrowing of the FWHM of the D peak from ~295 cm^{-1} to 281 cm^{-1}, respectively (Table 5). It was demonstrated that the reduction in

the D band width indicates the reduced structural disorder and formation of more ordered sp^2 C=C clusters in metal-doped DLC films [16,24,26].

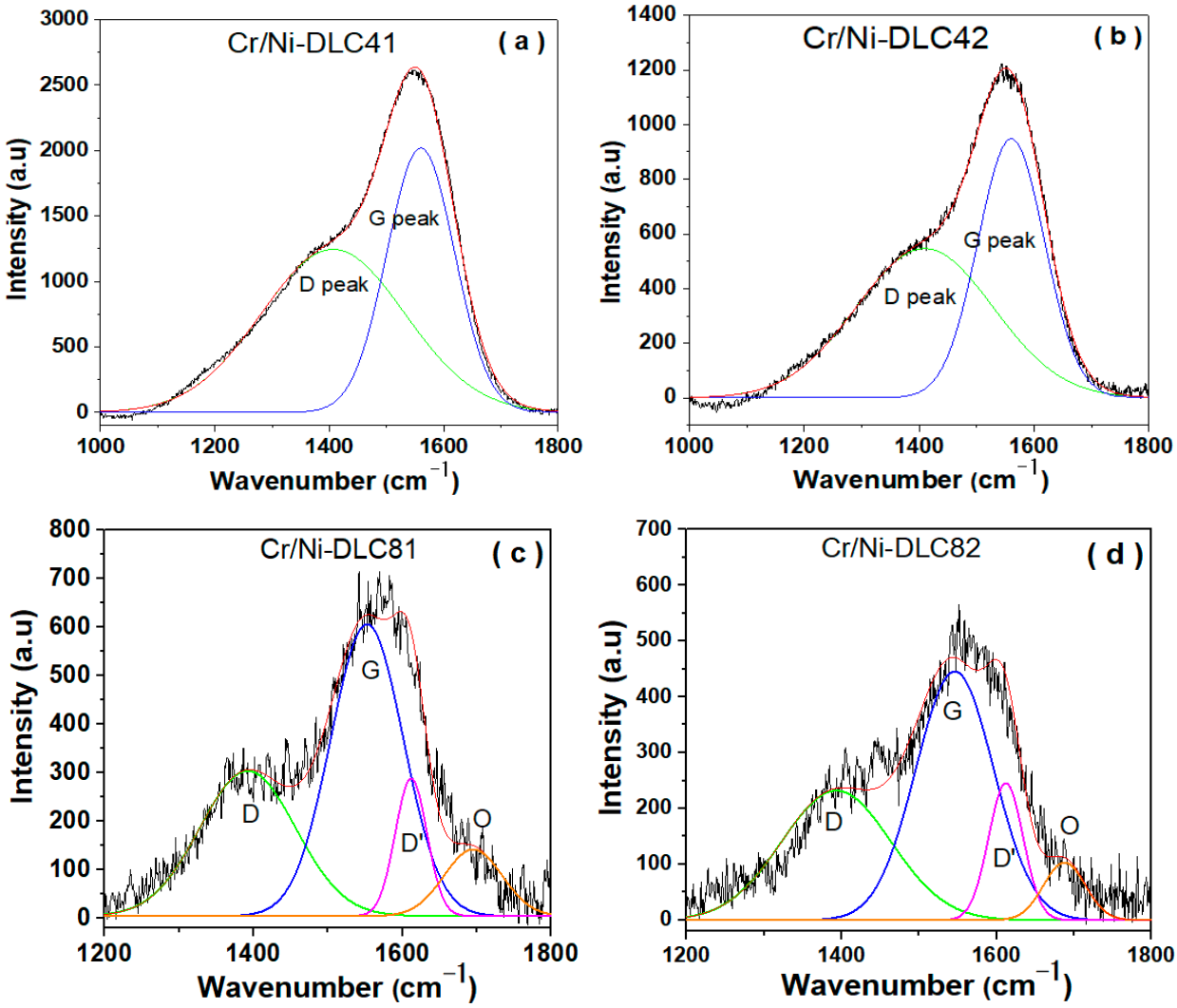

Figure 3. Raman spectra of (**a**) Cr/Ni-DLC41; (**b**) Cr/Ni-DLC42; (**c**) Cr/Ni-DLC81; and (**d**) Cr/Ni-DLC82 films.

The Cr/Ni-DLC41 film contains approximately 6.1 at.% of Cr and Ni dopants combined, whereas the Cr/Ni-DLC81 film has a higher content of 8.7 at.% of these dopants. The oxygen content in the Cr/Ni-DLC42 film was higher due to an increase in the total metal concentration (Table 1). The reduction in the formation temperature drastically changed the structure of the sputtered films. The shape of the Raman spectra of the Cr/Ni-DLC films synthesized at 185 °C, besides the traditional D and G peaks, demonstrated the appearance of additional peaks (Figure 3c,d). The additional shoulder observed at ~1612 cm^{-1} is attributed to the D′ peak. Meanwhile, the peak at ~1690 cm^{-1} observed in Cr/Ni-DLC films is related to the formation of the carbon-oxygen sites in the DLC films. This peak demonstrates the vibrations of localized carbonyl (C=O) bonds formed when oxygen is incorporated into the DLC structure. This is direct evidence that the oxygen has chemically modified the carbon network during the synthesis and/or after deposition of the film [32,42].

The D and G peak positions of the Cr/Ni-DLC81 film were situated at 1392 cm^{-1} and 1553 cm^{-1}, respectively. The I_D/I_G ratio was 0.49, while the $FWHM_G$ value was 115 cm^{-1}. The slightly higher total metal content resulted only in slight changes in the

bonding microstructure of the films. The I_D/I_G ratio was increased to 0.52, while the G band and D peaks became slightly broader (Figure 3d). The D peak intensity was reduced, and the separation of the G and D peaks was induced with the reduction in temperature. It was stated that the separation of the D and G peaks in the DLC films is associated with the conversion of the sp^3 to sp^2 sites and an increase in the graphitization degree of DLC films [43]. Typically, the graphitization is induced with the increase in the substrate temperature [44], the addition of a high fraction of metal dopants or annealing of the DLC films [7,28,29]. R. Z. Moghadam et al. [45] demonstrated that the augmentation of the oxygen amount in the DLC coatings resulted in the separation of the D and G bands. The addition of oxygen usually increases the I_D/I_G ratio and leads to the narrowing of the G and D peaks for DLC films [46]. The appearance of the D' peak at ~1612 cm^{-1} in a DLC film corresponds to a blue-shifted G-band arising from ordered sp^2 (graphitic) carbon clusters. The appearance of the D' peak indicates a high fraction of graphitic clusters, and this band could arise due to higher deposition temperature, metal or oxygen doping or post-growth relaxation [41,45].

The increase in the temperature from 185 to 235 °C in both films increased the I_D/I_G ratios (Figure 3). However, the shape of the Raman spectra and the appearance of the additional peaks clearly demonstrated that the structural changes related to the transition of sp^3 bonds to sp^2 sites were induced at lower temperatures. This variation in the D and G peaks' intensity and area ratio is attributed to an increase in the size and number of sp^2-bonded carbon clusters and a decrease in sp^3 content, which indicates a higher disorder or formation of nano-crystalline graphite. These changes align with the deposition at higher temperatures [47]. The augmentation in the sp^2 bond amount with the increase in the metal content has been observed in other works from the literature, where Cu/Cr co-dopants [23] or Mo, Ag, Ag/Ti dopants were used [9,41,48]. Meanwhile, the Raman spectroscopy demonstrated that only slight structural changes were observed between the films deposited at the same temperature. The increase in the metal amounts when the Cr/Ni-DLC coatings were prepared at 235 °C resulted in only a slight increase in the fraction of sp^2 C=C bonds (according to Raman data such as I_D/I_G ratio, G peak position and $FWHM_G$), but the sp^3 content remained similar and a reduction in the carbon oxide bonds was observed (from XPS data). Despite the increase in the oxygen content in Cr/Ni-DLC42 film, most of the oxygen was bonded with chromium and nickel, which partially inhibited the formation of carbon-oxygen bonds and prevented disruption of the sp^3 C-C network. D. Zhang et al. [25] observed that the I_D/I_G ratio trend in Ag or Ag/Cr doped a-C films depended not only on the type of doped metals and concentration, but also on the initial structure of carbon coatings. Typically, the increase in Ni or Cr content in DLC films results in higher content of the sp^2 sites and formation of larger size graphite clusters due to the catalytic role of Ni and Cr [13,15,19,24,25,34]. However, the formation of chromium oxides instead of the metallic chromium in the DLC matrix can inhibit the graphitization process. Most likely, the suppression of sp^3 bond destruction was partly induced when the Cr/Ni-DLC42 film was formed, as only minor changes in the A_D/A_G and I_D/I_G ratios and in the G peak positions were observed.

3.2. Surface Morphology

The 3D images of the film's surfaces, measured using AFM, demonstrate homogeneous surface morphology (Figure 4). The Cr/Ni-DLC films had a cauliflower-like morphology. The average surface roughness (R_a) of the Cr/Ni-DLC films deposited at 235 °C insignificantly increased from 0.83 nm to 0.88 nm with the increase in metal content, respectively. The reduction in the synthesis temperature almost had no effect on the surface roughness, as R_a values were 0.84 nm and 0.87 nm for the Cr/Ni-DLC81 and Cr/Ni-DLC82 films,

respectively. The root mean square roughness (R_q) values were 1.08 nm, 1.13 nm, 1.11 nm and 1.18 nm for Cr/Ni-DLC41, Cr/Ni-DLC42, Cr/Ni-DLC81 and Cr/Ni-DLC82 films, respectively. Notably, the R_q value for the silicon substrate was 0.7 nm, confirming a very smooth starting surface. As the deposition temperature rose from 185 to 235 °C, the R_a and R_q values of the Cr/Ni-DLC films formed at the same shield openings were slightly lower. This small difference of about 3% with the deposition temperature changes indicates that the surface roughness does not play a significant role in the observed tribological behavior. Instead, the reduction in the friction coefficient at a higher deposition temperature is mainly attributed to changes in the bonding structure, as supported by XPS and Raman results.

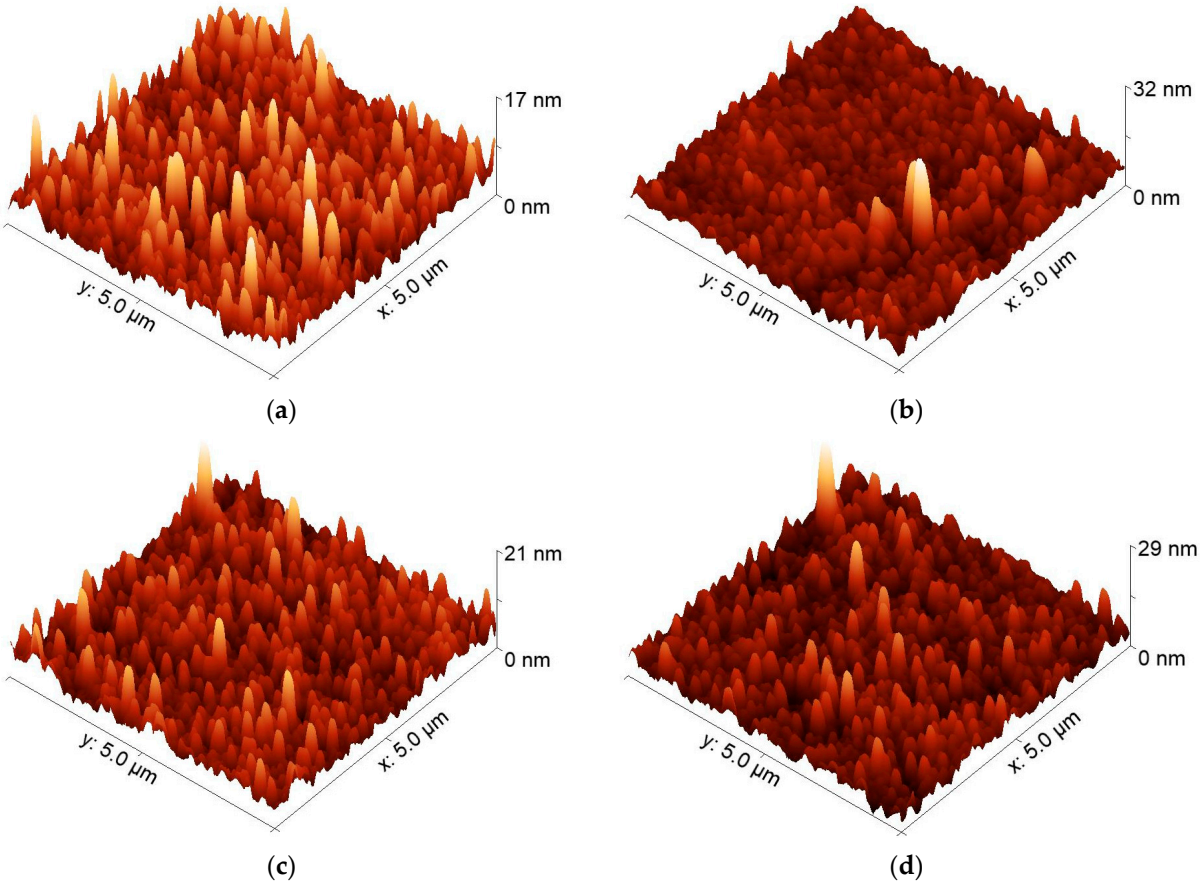

Figure 4. Morphology of the films synthesized at (**a**,**b**) 235 °C and (**c**,**d**) 185 °C, (**a**) Cr/Ni-DLC41, (**b**) Cr/Ni-DLC42, (**c**) Cr/Ni-DLC81 and (**d**) Cr/Ni-DLC82.

A similar observation was found in our previous study [9], where the incorporation of Mo dopant into DLC films resulted in lower surface roughness values. However, the change in temperature deposition at that amount of Mo did not show a significant effect on the surface roughness of the film. It should be noted that the undoped DLC films in our previous work [9] exhibited a slight reduction in the surface roughness with the deposition temperature, where the values decreased from 2.5 to 1.5 nm for R_a. Notably, the deposition temperature effect was rarely studied in the literature, where most research focuses on hardness, friction and wear behavior [35,48–50].

The thickness of the Cr/Ni-DLC films deposited at 235 °C was slightly higher, but the roughness was lower than that of the films sputtered at 185 °C. When the distance increases, the sputtered atoms travel a longer path through the plasma, undergo more collisions with gas molecules and lose more kinetic energy before reaching the Si substrate. Thus, the carbon, chromium and nickel atoms arrive with less kinetic energy, so the Cr/Ni-DLC

film grows with lower surface diffusion of adatoms and densification, producing a slightly rougher and more porous structure. L. Sun et al. [24] demonstrated that the increase in the target sputtering current resulted in a higher growth rate of Cu/Cr-DLC films, but the surface roughness could be reduced due to increased energy of the arriving metal and carbon atoms.

3.3. Tribological and Mechanical Properties

The dependence of the friction force versus applied loads for the Cr/Ni-DLC films is given in Figure 5. The lowest friction force values were determined for the Cr/Ni-DLC42 film. As the applied load increased from 10 nN to 45 nN, the friction force linearly rose from 31 to 51 nN, respectively. The slight increase in the friction force was determined for the Cr/Ni-DLC41 film (Figure 5a). The friction forces of the Cr/Ni-DLC films were drastically enhanced as the deposition temperature was reduced from 235 to 180 °C. The friction force of the Cr/Ni-DLC81 film increased from 40 nN to 100 nN with an augmentation in the applied load (Figure 5a). The highest friction force values were determined for the Cr/Ni-DLC82 film. The applied force was used to calculate the friction coefficient values of Cr/Ni-DLC films, which are shown in Figure 5b.

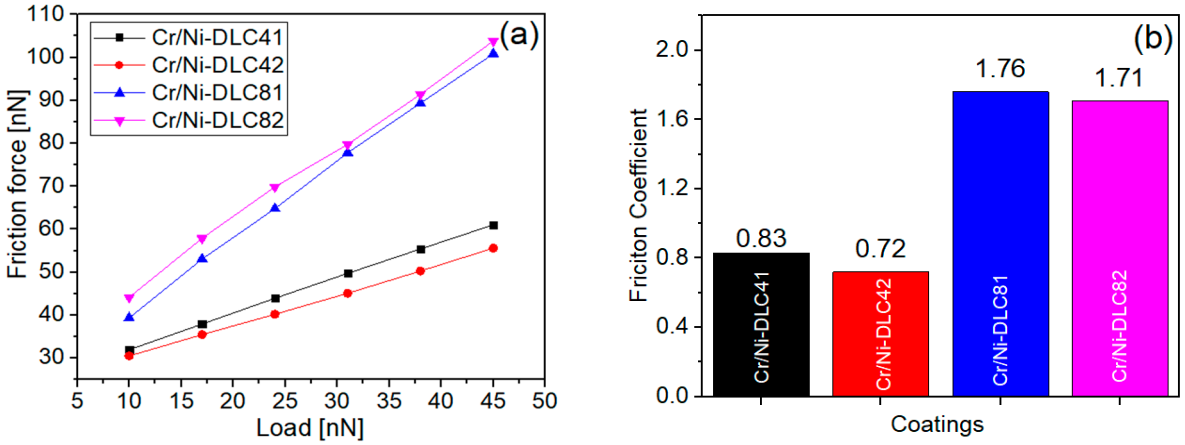

Figure 5. (**a**) Friction force as measured with AFM and (**b**) calculated friction coefficient of the coatings.

It can be seen that the friction force increased proportionally with the applied force (Figure 5a). The reduction in the friction coefficient from ~0.83 to ~0.72 was observed as the metal content increased when the deposition was done at 235 °C (Figure 5b). The reduction in the deposition temperature enhanced the friction coefficient of Cr/Ni-DLC films by more than twice. The highest friction coefficient (1.76) was obtained for the Cr/NiDLC81 film.

To interpret this change in the nanotribological behavior of films, the trend must be carefully analyzed in light of other findings from the literature. Theoretically, and based on other findings, different factors can affect the friction coefficient at the nanoscale range, such as surface roughness, the quantity of sp^2 C=C and sp^3 C-C sites, the nature and content of inserted dopants (both non-metal or metal), oxygen concentration, fraction of carbon-oxygen and metal–oxygen bonds obtained on the surface and the amount of metal carbides [10,23,28,35,41,47–51].

The surface roughness data and XPS measurements indicated that with increasing the deposition temperature, the surface roughness was slightly reduced (by 3%) also the formation of Ni-C or Cr-C sites was not detected. Thus, the friction coefficient reduction with the increase in the deposition temperature could be attributed mainly to the sp^2/sp^3 ratio, carbon and metal oxides groups on the film surface. Since surface roughness showed minimal change with deposition temperature, the observed reduction in friction coeffi-

cient at higher temperature cannot be attributed to topography alone. Instead, it directly correlates with the higher sp^3 fraction and lower C–O content of the films deposited at 235 °C. A higher sp^3 fraction provides a harder, more inert surface with reduced adhesive interactions and oxygen, which bonds more effectively with metals than with carbon, thus forming metal oxides rather than C–O/C=O bonds, further reducing the surface energy. These effects collectively explain the smoother sliding and reduced friction coefficient of the Cr/Ni-DLC films produced at higher temperatures. It was found that the surface energy of the DLC films is enhanced by the formation of metal oxide and carbon oxide bonds on the surface. However, the formation of carbon-oxygen bonds has a larger effect on enhancing the surface energy of DLC coatings compared to metal-oxide bonds [28,52–58]. L. Li et al. [55] demonstrated that the nanofriction force of Si-DLC films was reduced with the increase in Si content due to the enhancement in the sp^3 bond fraction. L. Bai et al. [56] found that an increase in surface roughness and a reduction in the sp^2 bond fraction enhanced the friction coefficient of DLC films, when a diamond tip and applied load in the range of 2.9 to 290 nN were used. F.S. Zhang et al. [57] observed that the friction coefficient of the DLC films increased with the addition of Ag when loads ranging from 10 μN to 80 μN were applied. The silver-doped DLC film exhibited the highest friction coefficient, along with the lowest surface roughness and the highest fraction of sp^2 bonds. L. Kolodziejczyk et al. [58] demonstrated that the friction coefficient of DLC films in the nanoscale range depends on the AFM tip type (Si or DLC), nature of dopant (Si or Ag) and Si or Ag concentration in the films. A. Amanov et al. [51] studied the tribological behavior of Si-DLC films at a similar deposition temperature range. The authors observed that the friction coefficient initially increased and then was reduced as the temperature rose from room temperature to 200 °C. This behavior can be assigned to the conversion of sp^3 C-C to sp^2 C=C with the increase in temperature. L. Sun et al. [23] studied Cu and Cr co-doped diamond-like carbon films at a broad deposition temperature range from 60 to 250 °C. They obtained an extremely low coefficient of friction, less than 0.11, for the films grown at 200 °C and 250 °C. The author attributed the friction performance to the formation of graphitization transfer film. Notably, the authors indicated the formation of the CrC phase in the films and the Cr-C fraction was increased, reaching 7 at.% at 250 °C. However, the reduction in the friction coefficient cannot be explained by changes in the sp^2/sp^3 bond ratios. B. Huang et al. [47] found that the O-Si-C bonds and graphite in a transfer layer can act as a lubricant, resulting in the reduction of the friction coefficient. Also, the C=O bonds that appeared on the Cr-DLC films' surface significantly influenced the lowering of the friction coefficient, as found by K. Weicheng et al. [10]. In addition, the increase in oxygen content is crucial in reducing the friction coefficient, as indicated by Y. Wang et al. [52]. Similar structural and tribological trends have been reported for magnetron-sputtered metal-doped DLC films, where bonding configuration and oxygen incorporation play a decisive role in determining mechanical and frictional behavior [53,59]. This explained our results, where the Cr/Ni-DLC42 film with the highest oxygen amount of 12.2 at.% (Table 1) demonstrated the lowest friction coefficient of 0.72 (Figure 5b).

Figure 6 illustrates the nanohardness (H) and Young's modulus (E) results of the films depending on the penetration depths, whereas the average data is provided in Table 6. The results indicated that the highest nanohardness and Young's modulus values of 5.69 and 63.4 GPa were observed for the Cr/Ni-DLC41 film. The increase in the metal and oxygen content reduced the nanohardness of the Cr/Ni-DLC film by 11%.

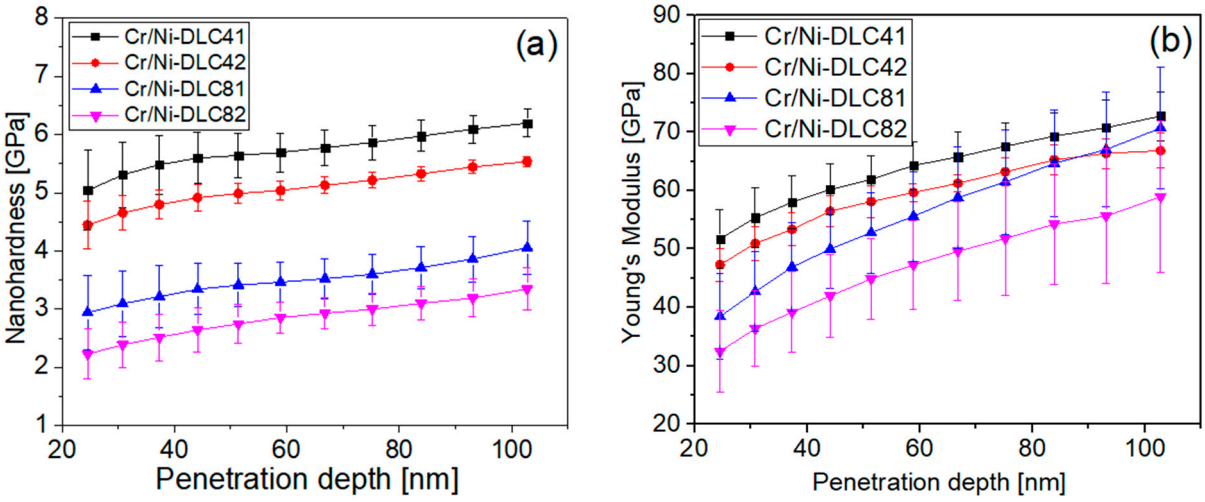

Figure 6. (**a**) Nanohardness and (**b**) Young's modulus of the deposited coatings.

Table 6. Mechanical properties of films derived by nanoindentation.

Samples	Hardness (H) [GPa]	Young's Modulus (E) [GPa]	H/E	H^3/E^2 [GPa]
Cr/Ni-DLC81	3.47 ± 0.44	55.37 ± 1.29	0.063 ± 0.006	0.014 ± 0.005
Cr/Ni-DLC82	2.81 ± 0.06	46.58 ± 2.20	0.060 ± 0.002	0.010 ± 0.001
Cr/Ni-DLC41	5.69 ± 0.15	63.42 ± 0.41	0.090 ± 0.002	0.046 ± 0.004
Cr/Ni-DLC42	5.04 ± 0.09	58.98 ± 0.52	0.086 ± 0.001	0.037 ± 0.002

Notably, the increase in the Young's modulus with the penetration depth was observed for all films, but it was more pronounced for the Cr/Ni-DLC81 film. Such trends are found when films formed are softer compared to the higher hardness substrate material. At shallow depths, the measurement is dominated by the top layer, which contains higher fractions of sp^2 and C–O bonds, resulting in a lower apparent modulus. With increasing penetration depth, the indenter probes beyond this compliant surface layer and the contribution from the underlying dense carbon matrix and the stiff silicon substrate becomes more pronounced, leading to a higher measured value. This depth effect is more visible in the softer Cr/Ni-DLC films deposited at lower temperatures, whereas the harder sp^3-rich films deposited at 235 °C show a more stable Young's modulus value response with increasing depth.

The Cr/Ni-DLC coatings exhibited a significant reduction in the nanohardness and Young's modulus when the deposition temperature was reduced to 185 °C. The nanohardness of the Cr/Ni-DLC81 film was 3.47 GPa. The enhancement in the oxygen content in the co-doped film led to further reduction in the nanohardness down to 2.81 GPa. The decrease in the temperature resulted not only in a decrease in the hardness, but also in the lower Young's modulus values. The average Young's modulus of Cr/Ni-DLC films decreased from ~55.4 to ~46.6 GPa when the metal content was enhanced. This change aligns with L. Sun et al. [23] findings, where the hardness of the Cr/Cu-DLC coatings increased with the synthesis temperature, their values rose continuously from 10.5 to 19.2 GPa between 100 and 250 °C. The authors explained this trend by two reasons, first the formation of chromium carbides, which may increase the hardness of DLC films, and the graphitization, which decreases the DLC films' hardness. However, when the concentration of the Cu/Cr decreased with deposition temperature, this led to less disorder in the DLC lattice and resulted in the increased hardness of films. B. Zhou et al. [34] indicated that the hardness of the Cr/Ni-DLC films increased as the sp^3/sp^2 ratio was enhanced and the fraction of Cr-C

bonds was reduced. It was observed that the mechanical properties (hardness and Young's modulus) of the Cr-DLC films increased with the addition of a moderate amount (up to 15 at.%) of Cr, reaching the hardness of ~4.5 GPa [16]. The increase in the hardness with the addition of Cr was related to the emergence of Cr-O and Cr-C bonds instead of C-O and C=O sites in the pure DLC films, which resulted in a higher fraction of sp^3 bonds in Cr-DLC films. A.A. Solovyev et al. [19] demonstrated that the hardness of the Ni-DLC films was reduced from 10.28 to 3.79 GPa when the Ni concentration was increased from 25 to 58 at.%, respectively. The reduction in the nanohardness was attributed to the increase in sp^2 site fraction, oxidation, formation of Ni-O sites and Ni_3C crystallites in the carbon matrix.

The calculated H/E and H^3/E^2 ratios for Cr/Ni-DLC films are shown in Table 6. The increase in Cr/Ni co-dopant concentration in the DLC film formed at 235 °C reduced the H/E ratio from 0.090 to 0.086 GPa, respectively. Meanwhile, the H/E ratios were 0.063 and 0.060 for the Cr/Ni-DLC81 and Cr/Ni-DLC82 films, respectively. The highest H^3/E^2 ratio of 0.046 GPa was measured for the Cr/Ni-DLC41 film. The H^3/E^2 ratios were reduced more than three times with the reduction in temperature, which indicates a lower resistance to plastic deformation (Table 6). The higher H/E ratio values for the DLC or doped DLC films indicate a greater elastic recovery, better resistance to cracking, improved wear resistance and toughness [28,59]. The H^3/E^2 ratio is attributed to the resistance to plastic deformation. It was discovered that the Cr/Ni-DLC films formed at higher temperatures demonstrated much higher resistance to plastic deformation, as their H^3/E^2 ratios were much higher compared to those of films deposited at 185 °C. As Ni and Cr are plastic metals and have a strong plastic deformation ability at low content, they could enhance the hardness and toughness of the Cr/Ni-DLC films. However, the higher Cr or Ni content will enhance the sp^2 carbon site fraction and destroy the three-dimensional network of carbon, which reduces the hardness and H/E ratio.

XPS and Raman results showed that the films formed at 235 °C had a higher sp^3 content and more metallic Ni clusters, and their nanohardness was twice as high compared to the Cr/Ni-DLC films formed at 185 °C. The larger Cr/Ni metal amount resulted in higher oxygen concentration in the films and led to the reduction in the sp^3 sites and increased the fraction of C-O and C=O sites. The nanohardness in metal-doped DLC films was reduced as the fraction of the sp^3 bonds was transformed to sp^2 C=C or an increase in the C-O and C=O sites was obtained in metal-doped DLC films [14,23]. B. Huang et al. [47] investigated the effect of deposition temperature on Si-DLC films. Two different tendencies were found depending on the deposition temperature range. The Si-DLC films' toughness was enhanced by a formation temperature ranging from 60 to 120 °C. However, a deposition temperature higher than 120 °C causes a decrease in hardness. The authors attributed the increase in hardness to the generation of sp^3, while the graphitization (formation of sp^2 bonds) weakened the films' hardness. The relatively low hardness obtained in this study is attributed to the sputtering technique used and the relatively high pressure in the vacuum chamber. However, the control of the substrate temperature and Cr/Ni concentrations allowed for the management of the oxygen concentration and sp^2/sp^3 ratio in the DLC films.

Figure 7a presents a three-dimensional surface view of scratches formed on the surface of the Cr/Ni-DLC41 film, serving as a representative example. It demonstrates the progressive increase in scratch depth along the trajectory, reaching a maximum at the end of the scratch path. Figure 7b displays the scratch profiles on the Cr/Ni-DLC41 film at the end of the trajectories for applied loads ranging from 3 to 7 μN. Figure 7c,d illustrates the variation in scratch depth and width versus the applied load for Cr/Ni-DLC films.

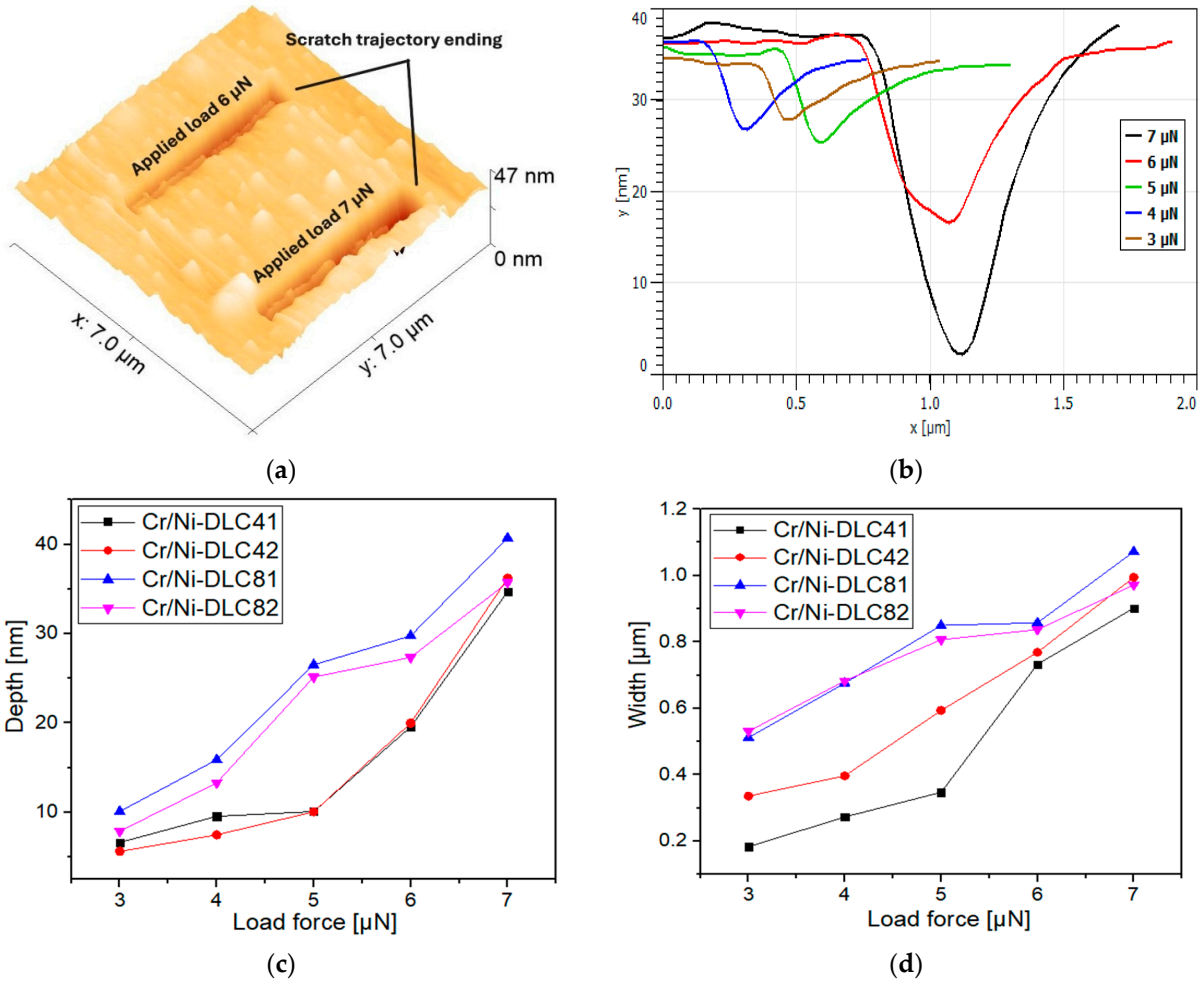

Figure 7. (**a**) surface morphology of Cr/Ni-DLC41 film after scratching, (**b**) scratch profiles of each load force on the Cr/Ni-DLC41 film at the end of the scratch trajectory, (**c**,**d**) variation in depth and width of the scratches versus the load forces of the films.

The results show a clear trend: both the depth and width of the scratches increased with the increase in the applied force. Specifically, the scratch depth ranges from approximately 5 to 40 nm, while the width varies between 0.2 and 1.1 µm depending on the measured Cr/Ni-DLC film. It should be highlighted that the Cr/Ni-DLC81 film demonstrated the lowest scratch-resistant behavior. The increase of the load force from 3 to 7 µm enhanced the groove depth and width from 10 to 40 nm and 0.5 to 1.1 µm, respectively. Importantly, the scratches remain confined within the film, not penetrating the silicon substrate, consistent with the film thicknesses, which range from 160 to 180 nm [9]. Furthermore, the data reveal that both the scratch depth and width decrease with increasing deposition temperature, regardless of the applied load. This observation aligns with nanoindentation results, which indicate that raising the temperature from 185 °C to 235 °C enhances the surface hardness of the films and improves their resistance to scratching. Thus, the groove depth and width of Cr/Ni-DLC41 film, due to the highest hardness value, varied from ~6 to 35 nm and 0.2 to 0.9 µm, respectively. However, this improvement becomes less pronounced at the highest applied load of 7 µN, as the differences in depth and width of scratches across different deposition temperatures begin to converge, as shown in Figure 7c,d. Notably, for the Cr/Ni-DLC41 and Cr/Ni-DLC42 films deposited at higher temperatures, the increase in scratch depth is initially gradual between 3 and 5 µN, followed by a more rapid rise beyond 5 µN of load force. This behavior may be attributed to the presence of higher concentrations of metal oxides and carbon oxides near the surface, as indicated by XPS analysis.

The improvement in hardness and Young's modulus at 235 °C is directly linked to the higher sp^3 content. Tetrahedral carbon bonds provide stronger cross-linking and higher resistance to plastic deformation compared to sp^2 bonds. At lower deposition temperature, higher metal oxidation and oxygen concentrations destabilize the sp^3 network, leading to the formation of softer Cr/Ni-DLC films with more graphitic bonds and less disordered sp^2 bonds.

Several results were obtained in the literature [60], comparable results were reported by L. Vieira et al. [61], who conducted the nanoscale scratch testing on silver-doped DLC films deposited on silicon substrates under an applied force of up to 30 μN. They observed similar V-shaped scratch profiles with widths around 100 nm and depths of approximately 4.7 nm. X. Jiang et al. [62] obtained quite perfect V-shaped scratches, where the groove width and depth increased with the applied load. The authors discovered the potential of using a DLC-coated tip to create nanopatterns on hard surfaces, such as silicon, in a convenient manner. Additionally, S. Miyake et al. [63] analyzed the scratch behavior of ultra-thin DLC films (up to 5 nm thick) deposited via different techniques, attributing variations in scratch performance to differences in film hardness. A.A. Tseng [64] observed that the higher hardness of the different materials resulted in the formation of narrower and shallower grooves during the scratch tests. We found that the scratch test results further confirmed the nanohardness data and correlated with the Raman and XPS results. The Cr/Ni-DLC films with a higher sp^3 fraction demonstrated a lower penetration of grooves and narrower scratches under the same applied loads. Thus, the mechanical property trends are a direct manifestation of the temperature-driven control of sp^2/sp^3 bonding and oxygen concentration in the Cr/Ni-DLC films.

4. Conclusions

Chromium and nickel co-doped DLC films were successfully synthesized by magnetron sputtering at two deposition temperatures, 185 °C and 235 °C. The results demonstrate that the deposition temperature is a key parameter controlling dopant incorporation, bonding structure and the resulting mechanical and nanotribological performance of the Cr/Ni-DLC films. At a lower deposition temperature of 185 °C, higher concentrations of Ni/Cr and oxygen were incorporated into the coatings. Both factors promoted the transformation of sp^3 C-C sites towards sp^2 carbon bonding and clustering of sp^2 sites: Ni and Cr metals acted as graphitization catalysts, while oxygen bound directly to carbon (C–O, C=O) and metals (Ni-O, Cr-O) disrupted the tetrahedral carbon network. As a result, the Cr/Ni-DLC films exhibited higher sp^2/sp^3 ratios, lower hardness, Young's modulus and increased friction coefficients.

In contrast, a rise in the formation temperature of up to 235 °C enhanced the mobility of arriving adatoms, reduced the oxygen concentration, enhanced the metallic Ni fraction and promoted preferential oxygen bonding with metals, forming Ni–O and Cr–O instead of C–O or C=O sites. These effects collectively stabilized sp^3 C-C bonding, leading to a lower sp^2/sp^3 ratio and slightly reducing the surface roughness of Cr/Ni-DLC films. Consequently, the films deposited at 235 °C showed a superior hardness of 5.69 GPa, a higher Young's modulus (up to 63.4 GPa), improved resistance to scratch loads and the friction coefficient was reduced by 2.4 times. The formation of the metal carbide bonds in Cr/Ni-DLC films was not observed under the used synthesis temperatures and Cr/Ni concentrations.

Therefore, the mechanism of temperature-driven enhancement can be summarized as follows: a higher deposition temperature facilitates the diffusion of atoms on the surface and modifies dopant/oxygen chemistry, which suppresses the formation of sp^2 C=C and oxygen-carbon sites and favors the stabilization of sp^3 bonding in the Cr/Ni-DLC films.

This microstructural control directly results in the improved hardness, toughness and tribological performance of Cr/Ni-DLC films. The moderate thermal activation stabilizes the amorphous carbon network through preferential metal–oxygen bonding and allows for controlling the graphitization level during the growth of Cr/Ni co-doped DLC films.

These findings not only clarify the role of deposition temperature in tailoring the microstructure and mechanical properties of Cr/Ni-DLC films but also provide a mechanistic framework for designing other multi-element co-doped DLC coatings with optimized sp^2/sp^3 ratios and dopant concentrations for advanced protective applications.

Author Contributions: Conceptualization, L.M. and H.Z.; methodology, H.Z. and L.M.; software, H.K., E.V. and A.Š.; validation, H.Z. and L.M.; formal analysis, H.Z., H.K., E.G., E.V. and A.Š.; investigation, H.Z.; resources, L.M.; data curation, H.Z.; writing—original draft preparation, H.Z. and L.M.; writing—review and editing, H.Z. and L.M.; visualization, H.Z., H.K., E.G. and A.Š.; supervision, L.M. All authors have read and agreed to the published version of the manuscript.

Funding: This research received no external funding.

Data Availability Statement: Data are contained within this article.

Acknowledgments: The support of the Strategic Program Excellence Initiative at the Jagiellonian University SciMat (Grant No. U1U/P05/NO/01.05) and of the Polish National Science Center (NCN) (OPUS Grant No. UMO/2021/43/B/ST5/00705) is gratefully acknowledged by H.K. and E.G. This article is partly based upon work from COST Action CA23155, supported by COST (European Cooperation in Science and Technology). We are thankful to the Institute of Solid State Physics, University of Latvia, as the Centre of Excellence has received funding from the European Union's Horizon 2020 Framework Programme H2020-WIDESPREAD-01-2016-2017-TeamingPhase2 under grant agreement No. 739508, project CAMART2.

Conflicts of Interest: The authors declare no conflicts of interest.

References

1. Barba, E.; Claver, A.; Montalà, F.; Palacio, J.F.; Luis-Pérez, C.J.; Sala, N.; Colominas, C.; García, J.A. Study of the Industrial Application of Diamond-Like Carbon Coatings Deposited on Advanced Tool Steels. *Coatings* **2024**, *14*, 159. [CrossRef]
2. Kolawole, F.O.; Kolade, O.S.; Bello, S.A.; Kolawole, S.K.; Ayeni, A.T.; Elijah, T.F.; Borisade, S.G.; Tschiptschin, A.P. The improvement of diamond-like carbon coatings for tribological and tribo-corrosion applications in automobile engines: An updated review study. *Int. J. Adv. Manuf. Technol.* **2023**, *126*, 2295–2322. [CrossRef]
3. Peng, Y.; Peng, J.; Wang, Z.; Xiao, Y.; Qiu, X. Diamond-like Carbon Coatings in the Biomedical Field: Properties, Applications and Future Development. *Coatings* **2022**, *12*, 1088. [CrossRef]
4. Shah, R.; Pai, N.; Khandekar, R.; Aslam, R.; Wang, Q.; Yan, Z.; Rosenkranz, A. DLC coatings in biomedical applications—Review on current advantages, existing challenges, and future directions. *Surf. Coat. Technol.* **2024**, *487*, 131006. [CrossRef]
5. Wang, P.; Wang, X.; Xu, T.; Liu, W.; Zhang, J. Comparing internal stress in diamond-like carbon films with different structure. *Thin Solid Film.* **2007**, *515*, 6899–6903. [CrossRef]
6. Ban, M.; Hasegawa, T.; Fujii, S.; Fujioka, J. Stress and structural properties of diamond-like carbon films deposited by electron beam excited plasma CVD. *Diam. Relat. Mater.* **2003**, *12*, 47–56. [CrossRef]
7. Vetter, J. 60 years of DLC coatings: Historical highlights and technical review of cathodic arc processes to synthesize various DLC types, and their evolution for industrial applications. *Surf. Coat. Technol.* **2014**, *257*, 213–240. [CrossRef]
8. Kalin, M.; Roman, E.; Ožbolt, L.; Vižintin, J. Metal-doped (Ti, WC) diamond-like-carbon coatings: Reactions with extreme-pressure oil additives under tribological and static conditions. *Thin Solid Film.* **2010**, *518*, 4336–4344. [CrossRef]
9. Zhairabany, H.; Khaksar, H.; Vanags, E.; Marcinauskas, L. Effect of Molybdenum Concentration and Deposition Temperature on the Structure and Tribological Properties of the Diamond-like Carbon Films. *Crystals* **2024**, *14*, 962. [CrossRef]
10. Weicheng, K.; Zhou, Y.; Jun, H. Effect of carburizing treatment on microstructural, mechanical and tribological performances of Cr doped DLC coating deposited on Ti6Al4V alloy. *Ceram. Int.* **2021**, *47*, 34425–34436. [CrossRef]
11. Mi, B.; Wang, H.; Wang, Q.; Cai, J.; Qin, Z.; Chen, Z. Corrosion resistance and contact resistance properties of Cr-doped amorphous carbon films deposited under different carbon target current on the 316L stainless steel bipolar plate for PEMFC. *Vacuum* **2022**, *203*, 111263. [CrossRef]

12. Wang, L.; Wu, Y.; Yu, S.; Liu, Y.; Shi, B.; Hu, E.; Hei, H. Investigation of hydrophobic and anti-corrosive behavior of Cr-DLC film on stainless steel bipolar plate. *Diam. Relat. Mater.* **2022**, *129*, 109352. [CrossRef]
13. Zou, C.W.; Wang, H.J.; Feng, L.; Xue, S.W. Effects of Cr concentrations on the microstructure, hardness, and temperature-dependent tribological properties of Cr-DLC coatings. *Appl. Surf. Sci.* **2013**, *286*, 137–141. [CrossRef]
14. Gayathri, S.; Kumar, N.; Krishnan, R.; Ravindran, T.R.; Dash, S.; Tyagi, A.K.; Sridharan, M. Influence of Cr content on the micro-structural and tribological properties of PLD grown nanocomposite DLC-Cr thin films. *Mater. Chem. Phys.* **2015**, *167*, 194–200. [CrossRef]
15. Dovydaitis, V.; Marcinauskas, L.; Ayala, P.; Gnecco, E.; Chimborazo, J.; Zhairabany, H.; Zabels, R. The influence of Cr and Ni doping on the microstructure of oxygen containing diamond-like carbon films. *Vacuum* **2021**, *191*, 110351. [CrossRef]
16. Zhu, L.; Li, J.; Kang, J.; Tang, L.; Ma, G.; Han, C.; Shi, J.; Wang, H. Different Cr Contents on the Microstructure and Tribomechanical Properties of Multi-Layered Diamond-Like Carbon Films Prepared by Unbalanced Magnetron Sputtering. *J. Mater. Eng. Perform.* **2020**, *29*, 7131–7140. [CrossRef]
17. Khun, N.W.; Liu, E.; Yang, G.C. Structure, scratch resistance and corrosion performance of nickel doped diamond-like carbon thin films. *Surf. Coat. Technol.* **2010**, *204*, 3125–3130. [CrossRef]
18. Wang, X.; Zhang, X.; Hu, X.; Tian, Y.; Wang, H.; Fu, H.; Li, H. Molecular dynamics simulation of hybrid structure and mechanical properties of DLC/Ni-DLC thin films. *Sci. Rep.* **2024**, *14*, 18885. [CrossRef]
19. Solovyev, A.A.; Oskomov, K.V.; Grenadyorov, A.S.; Maloney, P.D. Preparation of nickel-containing conductive amorphous carbon films by magnetron sputtering with negative high-voltage pulsed substrate bias. *Thin Solid Film.* **2018**, *650*, 37–43. [CrossRef]
20. Xu, Y.; Sun, W.; Liu, E.; Zhou, M.; Zhang, B.; Cai, H.; Zhang, J. Effect of CNTs concentration on the microstructure and properties of B, Ni, CNTs co-doped diamond like carbon films. *Diam. Relat. Mater.* **2024**, *149*, 111526. [CrossRef]
21. Li, X.; Chen, C.S.; Tsao, C.C.; Hu, C.C.; Chen, C.; Hsu, C.Y. Characteristics of DLC films doped with multi-element alloy. *Int. J. Adv. Manuf. Technol.* **2022**, *121*, 2631–2646. [CrossRef]
22. Mi, B.; Wang, Q.; Xu, Y.; Qin, Z.; Chen, Z.; Wang, H. Improvement in Corrosion Resistance and Interfacial Contact Resistance Properties of 316L Stainless Steel by Coating with Cr, Ti Co-Doped Amorphous Carbon Films in the Environment of the PEMFCs. *Molecules* **2023**, *28*, 2821. [CrossRef]
23. Sun, L.; Zuo, X.; Guo, P.; Li, X.; Ke, P.; Wang, A. Role of deposition temperature on the mechanical and tribological properties of Cu and Cr co-doped diamond-like carbon films. *Thin Solid Film.* **2019**, *678*, 16–25. [CrossRef]
24. Sun, L.; Guo, P.; Ke, P.; Li, X.; Wang, A. Synergistic effect of Cu/Cr co-doping on the wettability and mechanical properties of diamond-like carbon films. *Diam. Relat. Mater.* **2016**, *68*, 1–9. [CrossRef]
25. Zhang, D.; Yi, P.; Peng, L.; Lai, X.; Pu, J. Amorphous carbon films doped with silver and chromium to achieve ultra-low interfacial electrical resistance and long-term durability in the application of proton exchange membrane fuel cells. *Carbon* **2019**, *145*, 333–344. [CrossRef]
26. Wu, Y.; Xu, Y.; Li, K.; Shi, B.; Liu, Y.; Gong, Y.; Yu, S. Comparation on the tribological properties of textured design between Si/Ni-DLC and Si/Ta-DLC composite films. *Vacuum* **2025**, *233*, 114017. [CrossRef]
27. Xiao, Y.; Sun, W.; Zhang, Y.; Jia, Y.; Liu, J.; Zhang, C. Electrodeposition, microstructure and tribological performance of Ni/(N) incorporated diamond-like carbon films. *Surf. Coat. Technol.* **2022**, *447*, 128876. [CrossRef]
28. Platnieks, O.; Zhairabany, H.; Khaksar, H.; Gnecco, E.; Gaidukovs, S.; Vanags, E.; Sarakovskis, A.; Marcinauskas, L. Deposition of silver and titanium co-doped diamond-like carbon films by magnetron sputtering. *Diam. Relat. Mater.* **2025**, *154*, 112200. [CrossRef]
29. Zhang, R.; Lee, W.Y.; Umehara, N.; Tokoroyama, T.; Murashima, M.; Takimoto, Y. The development of B/Cr co-doped DLC coating by FCVA deposition system and its tribological properties at 300 °C. *Surf. Coat. Technol.* **2024**, *487*, 130968. [CrossRef]
30. Zarei, A.; Momeni, M. Optical and structural properties of nitrogen incorporated Ni doped diamond-like carbon thin films. *Opt. Quantum Electron.* **2023**, *55*, 415. [CrossRef]
31. Dai, W.; Wu, L.; Wang, Q. Structure and Property of Diamond-like Carbon Coating with Si and O Co-Doping Deposited by Reactive Magnetron Sputtering. *J. Compos. Sci.* **2023**, *7*, 180. [CrossRef]
32. Zhang, Y.; Sun, W.; Dong, Y.; Ma, M.; Liu, Y.; Tian, S.; Xiao, Y.; Jia, Y. Electrodeposition and microstructure of Ni and B co-doped diamond-like carbon (Ni/B-DLC) films. *Surf. Coat. Technol.* **2021**, *405*, 126713. [CrossRef]
33. Zhou, C.; Ru, L.; Xiao, J.; Zhang, X.; Mo, X.; Jiang, A. Cr content regulates the friction and corrosion resistance of Cr/F-DLC thin films. *Diam. Relat. Mater.* **2025**, *157*, 112482. [CrossRef]
34. Zhou, B.; Piliptsou, D.G.; Jiang, X.; Rogachev, A.V.; Rudenkov, A.S.; Kulesh, E.A. Structure and mechanical properties of Ni and Cr binary doped amorphous carbon coatings deposited by magnetron sputtering and pulse cathodic arc. *Thin Solid Film.* **2020**, *701*, 137942. [CrossRef]
35. Zeng, Q.; Ning, Z. High-temperature tribological properties of diamond-like carbon films: A review. *Rev. Adv. Mater. Sci.* **2021**, *60*, 276–292. [CrossRef]

36. Zeng, Q. Thermally Induced Superlow Friction of DLC Films in Ambient Air. *High. Temp. Mater. Process* **2018**, *37*, 725–731. [CrossRef]
37. Qiang, L.; Gao, K.; Zhang, L.; Wang, J.; Zhang, B.; Zhang, J. Further improving the mechanical and tribological properties of low content Ti-doped DLC film by W incorporating. *Appl. Surf. Sci.* **2015**, *353*, 522–529. [CrossRef]
38. Zhou, H.; Hou, Q.; Xiao, T.; Wang, Y.; Liao, B.; Zhang, X. The composition, microstructure and mechanical properties of Ni/DLC nanocomposite films by filtered cathodic vacuum arc deposition. *Diam. Relat. Mater.* **2017**, *75*, 96–104. [CrossRef]
39. Yetim, A.F.; Kovacı, H.; Kasapoğlu, A.E.; Bozkurt, Y.B.; Çelik, A. Influences of Ti, Al and V metal doping on the structural, mechanical and tribological properties of DLC films. *Diam. Relat. Mater.* **2021**, *120*, 108639. [CrossRef]
40. Písařík, P.; Jelínek, M.; Remsa, J.; Mikšovský, J.; Zemek, J.; Jurek, K.; Kubinová, Š.; Lukeš, J.; Šepitka, J. Antibacterial, mechanical and surface properties of Ag-DLC films prepared by dual PLD for medical applications. *Mater. Sci. Eng. C* **2017**, *77*, 955–962. [CrossRef]
41. Marcinauskas, L.; Grigonis, A.; Valatkevicius, P.; Medvid, A. Irradiation of the graphite-like carbon films by ns-laser pulse. *Appl. Surf. Sci.* **2012**, *261*, 488–492. [CrossRef]
42. Nakamura, M.; Takagawa, Y.; Miura, K.; Kobata, J.; Zhu, W.; Nishiike, N.; Arao, K.; Marin, E.; Pezzotti, G. Structural alteration induced by substrate bias voltage variation in diamond-like carbon films fabricated by unbalanced magnetron sputtering. *Diam. Relat. Mater.* **2018**, *90*, 214–220. [CrossRef]
43. Khamnualthong, N.; Siangchaew, K.; Limsuwan, P. Thermal stability evaluation of diamond-like carbon for magnetic recording head application using raman spectroscopy. *Procedia Eng.* **2012**, *32*, 888–894. [CrossRef]
44. Zeng, H.; Zhang, Y.; Wu, Z.; Qin, Z.; Ji, H.; Liu, X.; Li, B.; Hu, W. Microstructure, magnetic properties and corrosion resistance of Co-DLC nanocomposite film controlled by substrate temperature. *Diam. Relat. Mater.* **2023**, *133*, 109673. [CrossRef]
45. Zarei Moghadam, R.; Ehsani, M.H.; Rezagholipour Dizaji, H.; Kameli, P.; Jannesari, M. Oxygen doping effect on wettability of diamond-like carbon films. *Mater. Res. Express* **2021**, *8*, 035601. [CrossRef]
46. Safaie, P.; Eshaghi, A.; Bakhshi, S.R. Structure and mechanical properties of oxygen doped diamond-like carbon thin films. *Diam. Relat. Mater.* **2016**, *70*, 91–97. [CrossRef]
47. Huang, B.; Liu, L.; Han, S.; Du, H.; Zhou, Q.; Zhang, E. Effect of deposition temperature on the microstructure and tribological properties of Si-DLC coatings prepared by PECVD. *Diam. Relat. Mater.* **2022**, *129*, 109345. [CrossRef]
48. Wu, Y.; Chen, J.; Li, H.; Ji, L.; Ye, Y.; Zhou, H. Preparation and properties of Ag/DLC nanocomposite films fabricated by unbalanced magnetron sputtering. *Appl. Surf. Sci.* **2013**, *284*, 165–170. [CrossRef]
49. Wang, X.; Zhang, X.; Wang, C.; Lu, Y.; Hao, J. High temperature tribology behavior of silicon and nitrogen doped hydrogenated diamond-like carbon (DLC) coatings. *Tribol. Int.* **2022**, *175*, 107845. [CrossRef]
50. Chen, Y.; Su, F.; Li, Q.; Sun, J.; Lin, S.; Ma, G. Extremely enhanced friction and wear performance of hydrogen-free DLC film at elevated temperatures via Si doping. *Tribol. Int.* **2024**, *199*, 109981. [CrossRef]
51. Amanov, A.; Watabe, T.; Tsuboi, R.; Sasaki, S. Improvement in the tribological characteristics of Si-DLC coating by laser surface texturing under oil-lubricated point contacts at various temperatures. *Surf. Coat. Technol.* **2013**, *232*, 549–560. [CrossRef]
52. Wang, Y.; Yin, Z.; Fan, D.; Bai, L. Friction behaviors of DLC films in an oxygen environment: An atomistic understanding from ReaxFF simulations. *Tribol. Int.* **2022**, *168*, 107448. [CrossRef]
53. Karslioglu, R.; Meletis, E.I. Synthesis, Characterization, and Wear Behavior of W-DLC Films Deposited on Si Substrates. *J. Nano Res.* **2023**, *81*, 105–120. [CrossRef]
54. Bîrleanu, C.; Pustan, M.; Șerdean, F.; Merie, V. AFM Nanotribomechanical Characterization of Thin Films for MEMS Applications. *Micromachines* **2022**, *13*, 23. [CrossRef]
55. Li, L.; Song, W.; Liu, J.; Liu, Q.; Wang, S.; Zhang, G. Nanomechanical and nanotribological behavior of ultra-thin silicon-doped diamond-like carbon films. *Tribol. Int.* **2016**, *94*, 616–623. [CrossRef]
56. Bai, L.; Srikanth, N.; Korznikova, E.A.; Baimova, J.A.; Dmitriev, S.V.; Zhou, K. Wear and friction between smooth or rough diamond-like carbon films and diamond tips. *Wear* **2017**, *372*, 12–20. [CrossRef]
57. Zhang, H.S.; Endrino, J.L.; Anders, A. Comparative surface and nano-tribological characteristics of nanocomposite diamond-like carbon thin films doped by silver. *Appl. Surf. Sci.* **2008**, *255*, 2551–2556. [CrossRef]
58. Kolodziejczyk, L.; Szymanski, W.; Batory, D.; Jedrzejczak, A. Nanotribology of silver and silicon doped carbon coatings. *Diam. Relat. Mater.* **2016**, *67*, 8–15. [CrossRef]
59. Liu, S.; Zhuang, W.; Ding, J.; Liu, Y.; Yu, W.; Yuan, J.; Zheng, J. Fabrication and Tribological Properties of Diamond-like Carbon Film with Cr Doping by High-Power Impulse Magnetron Sputtering. *Coatings* **2024**, *14*, 916. [CrossRef]
60. Yu, B.; Qian, L. Friction-Induced Nanofabrication: A Review. *Chin. J. Mech. Eng.* **2021**, *34*, 32. [CrossRef]
61. Vieira, L.; Lucas, F.L.C.; Fisssmer, S.F.; dos Santos, L.C.D.; Massi, M.; Leite, P.M.S.C.M.; Costa, C.A.R.; Lanzoni, E.M.; Pessoa, R.S.; Maciel, H.S. Scratch testing for micro- and nanoscale evaluation of tribocharging in DLC films containing silver nanoparticles using AFM and KPFM techniques. *Surf. Coat. Technol.* **2014**, *260*, 205–213. [CrossRef]

62. Jiang, X.; Wu, G.; Zhou, J.; Wang, S.; Tseng, A.A.; Du, Z. Nanopatterning on silicon surface using atomic force microscopy with diamond-like carbon (DLC)-coated Si probe. *Nanoscale Res. Lett.* **2011**, *6*, 1–7. [CrossRef]
63. Miyake, S.; Yamazaki, S. Nanoscratch properties of extremely thin diamond-like carbon films. *Wear* **2013**, *305*, 69–77. [CrossRef]
64. Tseng, A.A. A comparison study of scratch and wear properties using atomic force microscopy. *Appl. Surf. Sci.* **2010**, *256*, 4246–4252. [CrossRef]